The Astrophysical Journal, 971:8 (12pp), 2024 August 10 https://doi.org/10.3847/1538-4357/ad596b

Exploring the Archives: A Search for Novae in UVIT Snapshots of M31

Judhajeet Basu[1,2], Krishnendu S.[1,3], Sudhanshu Barway[1], Shatakshi Chamoli[1,2], and G. C. Anupama[1]
[1] Indian Institute of Astrophysics, 2nd Block Koramangala, 560034, Bangalore, India; judhajeet20@gmail.com
[2] Pondicherry University, R.V. Nagar, Kalapet, 605014 Puducherry, India
[3] Amrita School of Physical Sciences, Amrita School of Engineering, Amrita University, 641112, Ettimadai, India
Received 2024 May 3; revised 2024 June 12; accepted 2024 June 12; published 2024 August 1

Abstract

Extensive multiwavelength studies of novae have been carried out in our galaxy and in M31 for decades. However, UV studies of extragalactic novae are limited, especially those in quiescence. For the first time, we present a UV catalog of novae in M31 using the archival AstroSat Ultraviolet Imaging Telescope (UVIT) imaging data. We used two image subtraction techniques to retrieve objects located deep into the M31 central region. We have found 42 novae in total in the UVIT images, 15 of which have been detected in multiple filters in the far-ultraviolet (FUV) and near-ultraviolet. The novae detected at quiescence show signatures of accretion disk from their UV spectral energy distributions, whereas those in the outburst phase show signatures of a pseudo-photosphere. A few novae were also detected in multiple epochs. Some show a near-constant FUV magnitude at quiescence, while others caught near the outburst reveal pre-eruption dips in their light curves. We conclude with a discussion on the significance of UV surveys in illuminating theoretical predictions for novae systems, including detecting the elusive early UV flash.

Unified Astronomy Thesaurus concepts: Novae (1127); Andromeda Galaxy (39); Ultraviolet astronomy (1736); High energy astrophysics (739); Light curves (918); Spectral energy distribution (2129); Extinction (505); Accretion (14); Stellar accretion disks (1579); Astronomy image processing (2306); Transient detection (1957); Cataclysmic variable stars (203)

Materials only available in the online version of record: machine-readable tables

1. Introduction

Novae are cataclysmic events triggered by thermonuclear runaway reactions on the surface of accreting white dwarfs (WDs; Starrfield 1999; Bode & Evans 2008; Starrfield et al. 2016). These novae eruptions increase the brightness of the binary system up to several orders of magnitude, triggering nucleosynthesis and expelling material into the interstellar medium (ISM; Gehrz et al. 1998; Hernanz & Jose 1998). Individual novae are excellent laboratories for understanding accretion and mixing processes (Guo et al. 2022), binary evolution (Kraft 1964; Shen & Quataert 2022), supernova type Ia progenitors (Hillman et al. 2016; Wang 2018), and shock mechanisms (Aydi et al. 2020; Chomiuk et al. 2021). Nova studies are also important tracers of galactic chemical evolution and ISM enrichment (Starrfield et al. 2020).

One of the galaxies in which novae are studied in detail is M31, owing to its full visibility for more than half a year, close distance, low inclination, and high nova rate. High occurrences of recurrent novae (RNe) in M31, particularly those with short recurrence periods of fewer than 10 yr such as M31N 2008-12a[4] (Basu et al. 2024b), 2017-01e, 2013-10c, 1990-10a, 1963-09c, and others have intrigued astronomers and motivated them to explore the M31 galaxy. M31 has been surveyed extensively for novae for several decades in optical wave bands (Arp 1956; Rosino 1964, 1973; Ciardullo et al. 1987; Rosino et al. 1989; Sharov & Alksnis 1991; Tomaney & Shafter 1992; Rector et al. 1999; Shafter & Irby 2001; Darnley et al. 2004, 2006; Shafter et al. 2011b; Kasliwal et al. 2011; Lee et al. 2012; Williams et al. 2014, 2016; Rector et al. 2022). Over the past two decades, a few extensive studies have been performed in X-rays as well (Pietsch et al. 2007; Henze et al. 2010; Pietsch 2010; Henze et al. 2011, 2014). However, surveys are limited in the IR (Shafter et al. 2011a) and UV (Cao et al. 2012) bands. Quiescence studies of M31 novae were conducted by Williams et al. (2014, 2016) to look for progenitors using Hubble Space Telescope optical data, taking advantage of its high resolution.

Galactic novae have been studied in the UV since the launch of International Ultraviolet Explorer (Starrfield 1986 and references therein). Selvelli & Gilmozzi (2013) studied a sample of 18 galactic novae in quiescence in UV, focusing on their spectral energy distributions (SEDs), which were later combined with the outburst phase data by Selvelli & Gilmozzi (2019) for an overall understanding of the properties of old novae. Page et al. (2020, 2022) summarized the UV and X-ray light curves of galactic novae observed by Swift.

Rare UV studies of extragalactic novae, such as that of Cao et al. (2012) for M31, and those of Lessing et al. (2023) and Shara et al. (2023) for M87, concentrated primarily on eruption characteristics, spatial distribution, nova rates, and population studies. In the case of the Magellanic Clouds, their wide fields and low nova rates (Mróz et al. 2016) have led to limited surveys in optical and other bands. However, focusing on some individual novae, for instance, SMCN 2016-10a (Aydi et al. 2018), Nova LMC 1971b (Bode et al. 2016), and Nova LMC 1968 (Kuin et al. 2020) have revealed their UV quiescence features. Nonetheless, no study has been reported in the literature honing in on the systematic study of the quiescence phase of extragalactic novae in the UV. Though nova systems in M31 and other galaxies are expected to be similar to those in our Milky Way, the missing gap must be filled for completeness.

[4] All M31 novae designated as M31N YYYY-MMx will hereafter be denoted by YYYY-MMx.

This work presents the search for novae in M31 in the UV bands using archival AstroSat-Ultraviolet Imaging Telescope (UVIT) data. The paper discusses our data reduction, analysis, and detection methods and provides a catalog of the novae detected (including those caught during outbursts) as well as nondetection upper limits. We also briefly discuss the importance of UV missions and multiwavelength facilities as synoptic surveys for novae studies.

2. Data

2.1. Observations and Data Reduction

AstroSat is a space-based high-energy telescope in a low-inclination Earth orbit (Singh et al. 2014). UVIT is one of the primary instruments on board AstroSat, consisting of a twin telescope with one far-ultraviolet (FUV) and one near-ultraviolet (NUV)/visible channel, capable of observing simultaneously. Both telescopes have a mirror of 38 cm diameter and a circular field of view of 28′. UVIT has one of the best spatial resolutions at 1.″5 in the UV, making it suitable for studying extragalactic UV sources. UVIT's FUV filters offer a unique wave band (up to 1000 Å) to detect and study novae. Ground-based and in-orbit calibrations of the UVIT instrument are reported in Subramaniam et al. (2016) and Tandon et al. (2017a, 2017b).

UVIT has observed multiple fields of M31 in different filters over multiple epochs. The observations and data sets summarized by Leahy et al. (2020, 2021) are used in this work. Additional fields observed later by the same PI and other M31 fields observed by other PIs have also been looked into for this work. All the data utilized in this work have been summarized in Table 1. The `Level 1` and `Level 2` data have been made available online by the Indian Space Science Data Center's (ISSDC) *AstroBrowse*.[5] We obtained all the `L1` data and processed them using `CCDLAB` (Postma & Leahy 2017). The automated steps in `CCDLAB` include flat-fielding, drift correction, and cosmic-ray correction, among others discussed in detail in Postma & Leahy (2021). The orbit-wise images were registered and merged to get a single image with a high signal-to-noise ratio. The final step in `CCDLAB` involved performing astrometry on the merged and orbit-wise images.

The F148W images of all the 19 M31 fields were combined together to produce a composite image of M31 in the FUV. Individual images were normalized by their exposure times to bring them to the same scale. The normalized images were then tiled using `SWarp` (Bertin et al. 2002). The exposure array frames generated by `CCDLAB` were used as weights to take care of the edges and overlapping regions during tiling. The M31 FUV mosaic is shown in Figure 1.

2.2. Removal of Background Contribution from the Bulge

The bulge of M31 is shrouded by galactic light. This light contamination must be removed to search for any point source in this region. Since traditional image subtraction techniques do not entirely remove the light excess in crowded fields, we have used two methods to create templates for detecting novae in the bulge region.

The first method involves a median combination of multi-epoch images of the same field in the same filter. Tandon et al. (2020) showed that the sensitivity of the UVIT detectors has been constant over the years. Flux scaling of the multiepoch images thus only involved normalizing by their respective exposure times. Since UVIT is a space-based telescope, we expect the point-spread function (PSF) to be constant across all epochs; hence, PSF matching was not performed before combining the images. The flux-scaled images were registered and then median combined to make the template. This template was subtracted from the normalized image of each epoch to look for novae.

In the second method, we generated an isophote model of the bulge. We modeled the bulge of M31 by performing an isophote fit using the `isophote` module of the `photutils python` package (Bradley et al. 2023). The isophote model generated for a given range of semimajor axis (∼400 pixels = 2.′78) for each epoch was used as a template. Subtracting this template from its original image reveals all sources above the nuclear brightness level predicted by the model.

Both techniques were useful in detecting four novae, otherwise hidden in the bright M31 bulge. The difference images and the results from both methods are shown in Figure 2.

2.3. Source Detection and Photometry

A list of all M31 novae, as of 2022 May 19, is available at a website hosted by the Max Planck Institute for Extraterrestrial Physics[6] (Pietsch 2010). We performed forced photometry at the locations of the novae listed to check for their detection in the UVIT data. We also looked into novae that erupted after the latest UVIT observations (2020 November), for which the data are publicly available, to check for pre-eruption UV magnitudes or upper limits. All the detected novae were carefully inspected visually to confirm the detections. Sources in crowded fields, where source confusion could occur within a 5″ region of the nova, were rejected. We used a detection threshold of 3σ to eliminate faint sources. The limiting magnitude in the F148W filter for deep exposures (>10 ks) was found to be around 23 mag for a 3σ detection near the central region of M31. The detection limit for regions away from the center was around 0.5 mag deeper. The average limiting magnitude for each image is given in Table 1. However, it should be noted that the limiting magnitude varies spatially in an image. All the detected sources are shown in the UVIT F148W mosaic image in Figure 1, and their details are mentioned in Table 2.

Availability of multiple images in the same field and the same filter encouraged us to sum them and look for fainter novae in the deeper exposures. Summing the images increased the limiting magnitude of the images by 0.2–0.4 mag (see Table 1). We found three old novae, namely, 1985-09c, 1998-09e, and 2010-03a, in the coadded frame of the central region of M31. All three novae were fainter than 23 mag (see Table 2). The FUV and NUV magnitudes of detected novae and upper limits of all undetected novae in the deepest available images in each filter were estimated, and have been provided in the Appendix table.

Leahy et al. (2020) and Devaraj et al. (2023) found that the PSF of UVIT images is better represented by Moffat functions rather than an elliptical or circular Gaussian. However, neither a Moffat nor Gaussian PSF could accurately estimate the flux from stars, which was underestimated due to the presence of extended PSF wings in the UVIT images (Tandon et al. 2017b;

[5] https://astrobrowse.issdc.gov.in/astro_archive/archive/Home.jsp

[6] https://www.mpe.mpg.de/~m31novae/opt/m31/M31_table.html

Table 1
UVIT Observation Log of All Images, Including Coadded Frames, in Which at Least One Nova Was Detected

Observation ID	R.A. (deg)	Decl. (deg)	Filter	Field	Obs Epoch (BJD)	Exp Time (s)	Limiting Mag (AB mag)	Novae Detected
A02_028T01_9000000724	10.71683	41.12430	F148W	M31 01	2457671.85662	7736.347	22.94	18
A02_028T01_9000000724	10.71683	41.12430	F172M	M31 01	2457672.19496	3611.883	21.39	14
A02_028T01_9000000724	10.71683	41.12430	N219M	M31 01	2457671.85657	7780.686	22.08	12
A02_028T01_9000000724	10.71683	41.12430	N279N	M31 01	2457672.19491	3627.438	21.53	11
A07_007T04_9000003310	10.70412	41.27929	F148W	M31 01	2458805.25645	17045.731	23.37	17
A07_007T04_9000003310	10.70412	41.27929	F169M	M31 01	2458804.85075	10426.754	22.63	15
A07_007T04_9000003310	10.70412	41.27929	F172M	M31 01	2458806.27133	16606.192	22.34	15
A10_002T04_9000004022	10.59843	41.21609	F148W	M31 01	2459174.71396	11759.864	23.10	18
A02_028T03_9000000788	11.01776	41.54606	F148W	M31 02	2457704.13548	7942.829	22.69	3
A02_028T03_9000000788	11.01776	41.54606	F172M	M31 02	2457704.48574	5350.934	21.48	2
A02_028T03_9000000788	11.01776	41.54606	N219M	M31 02	2457704.13543	7986.231	22.01	2
A02_028T03_9000000788	11.01776	41.54606	N279N	M31 02	2457704.48567	5544.727	21.33	3
A10_002T05_9000004000	11.13728	41.48918	F148W	M31 02	2459167.97966	12610.195	22.77	1
A04_022T02_9000002184	11.33933	41.88125	F148W	M31 08	2458292.30948	3371.811	22.85	1
A04_022T02_9000002184	11.33933	41.88125	F172M	M31 08	2458292.98608	9017.513	22.29	1
A05_004T03_9000002508	9.87699	40.36606	F148W	M31 15	2458435.07551	4610.422	23.04	1
A05_004T03_9000002508	9.87699	40.36606	F169M	M31 15	2458435.27774	9286.96	22.69	1
A05_004T03_9000002538	9.86651	40.37805	F148W	M31 15	2458449.21674	2104.392	22.72	1
A05_004T03_9000002538	9.86651	40.37805	F169M	M31 15	2458449.42980	9224.752	22.76	1
Coadded frames[a]	10.70959[b]	41.27957[b]	F148W	M31 01	2458550.60901[c]	36541.942	23.54	3[d]
Coadded frames[a]	10.70959[b]	41.27957[b]	F172M	M31 01	2458239.23315[c]	20218.075	22.50	1[d]

Notes. The full table includes details of all individual and coadded frames analyzed in this work.
[a] Coadded frames include all the images of the same field in the same filter combined together. For example, the coadded frame of the M31 01 field in the F148W filter includes the sum of F148W images with Obs IDs A02_028T01_9000000724, A07_007T04_9000003310, and A10_002T04_9000004022.
[b] R.A. and decl. of the coadded frames are the centers of the coadded images.
[c] Observation epochs for coadded frames are the midpoint of the first and last observation.
[d] The number of novae detected in the coadded frames but not in the individual images.

(This table is available in its entirety in machine-readable form in the online article.)

Leahy et al. 2020). In such cases, aperture photometry gives the best results, but due to crowded fields of M31, aperture photometry is not a feasible solution. PSF photometry was performed using an elliptical Moffat function to fit the sources. Standard routines in `IRAF` (Tody 1993) were used for photometric measurements. To accurately measure the flux, we performed aperture photometry with an aperture of 15 pixels ($\sim 4 \times$ FWHM) and PSF photometry with a PSF radius of 11 pixels ($\sim 3 \times$ FWHM) of isolated bright sources to determine the aperture correction term. This correction took care of the emission from the extended PSF wings. It was then applied to the magnitudes of the novae obtained by PSF photometry. The zero-point calibrations in the AB system were adopted from Tandon et al. (2020). We have not corrected the magnitudes for extinction.

For the novae in the central fields, we tried aperture and PSF photometry on both sets of difference images. In aperture photometry, the background subtraction led to inconsistencies, whereas in PSF photometry, the PSF model fitting diverged. We thus performed PSF photometry with aperture correction of the bulge novae on the original science images using the same technique we used for the other novae. It ensured the measurements were consistent for all novae reported in this work.

The photometry of all the detected sources in various filters at different epochs is given in Table 3.

3. Results and Discussion

All the novae detected in the archival UVIT images are shown in Figure 1 and listed in Table 2. Nova outbursts can last for a wide range of duration, with a varied rate of decline (t_2 or t_3) of the light curve (Warner 2008). These parameters, in turn, depend on the physical nature of the system, i.e., the primary WD and the binary system. Theoretical models of Hachisu & Kato (2006) suggest the duration of the outburst depends on the WD mass and composition. Strope et al. (2010) studied the optical light curves of around 100 novae to look for various processes after the outburst capable of altering the light curve shapes. UV light curves have also been seen to vary in shape and duration. This is usually related to the supersoft X-ray phase (Page et al. 2022), which, in turn, is dependent on the WD mass (Hachisu & Kato 2006; Henze et al. 2011). Due to the wide spectrum of speed class of novae, we decided to take 100 days as the cutoff for novae in outburst, corresponding to a 7 mag decline from maxima for a 0.9 $M_{\odot}$ CO WD (Hachisu & Kato 2006). Additionally, considering pre-eruption dips and early UV flash, we consider novae detected within 20 days before the eruption to be in the outburst phase. For any other case, the detection is considered to be at quiescence.

Overall, we have detected 42 novae in various fields of M31 observed by UVIT. Almost 90% of the detected novae are concentrated within a $90' \times 90'$ region around the M31 center. This is expected because the nova rates follow the galactic light in optical/IR bands tracing the older stellar population of M31 (Rector et al. 2022). The following sections discuss the novae detected at different phases and their SEDs.

3.1. Novae Detected at Quiescence

Twenty-three novae were detected during quiescence, 21 of which were detected post-outburst. 2021-07d was detected

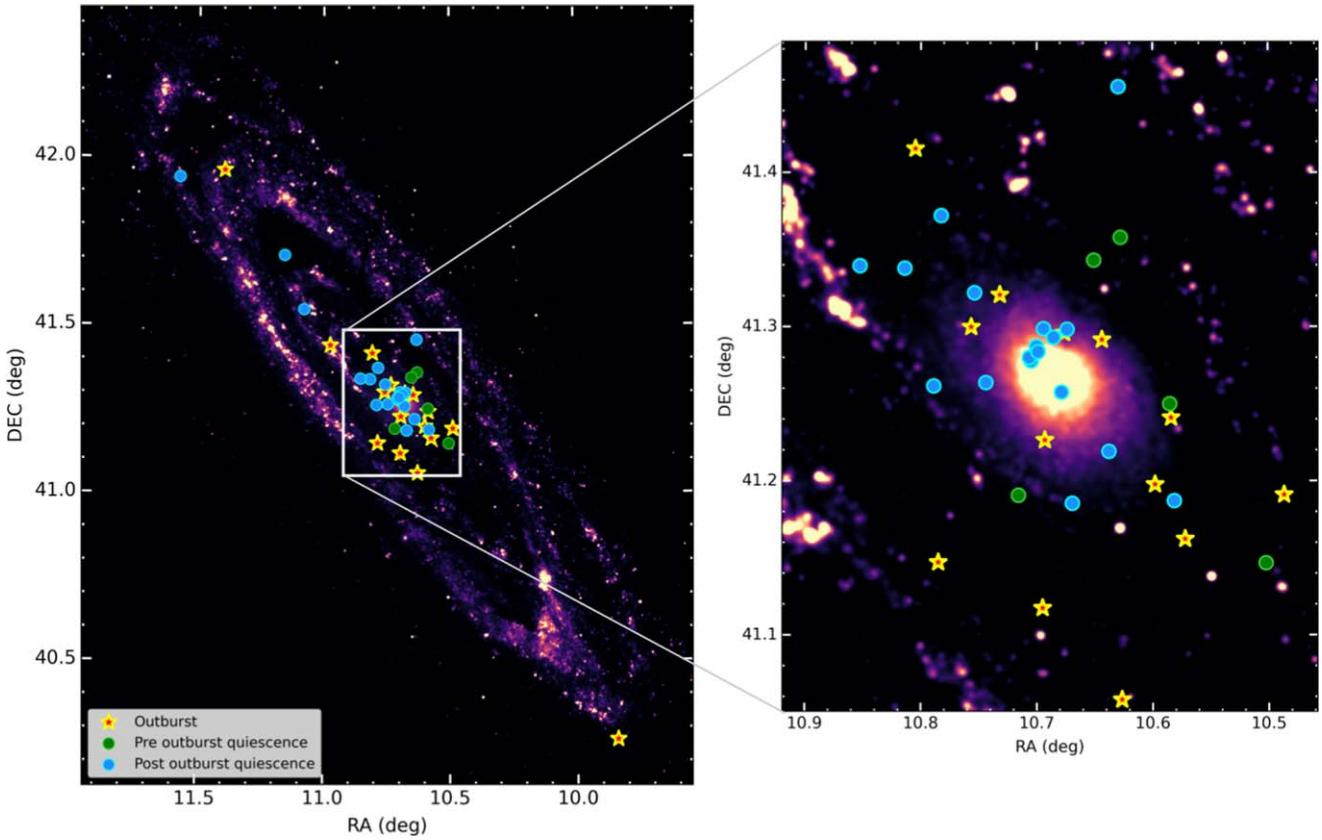

Figure 1. UVIT F148W mosaic image of M31 generated using `SWarp`. The locations of all the novae detected in the archival images are marked in the figure. The inset shows a zoomed-in version of the M31 central region.

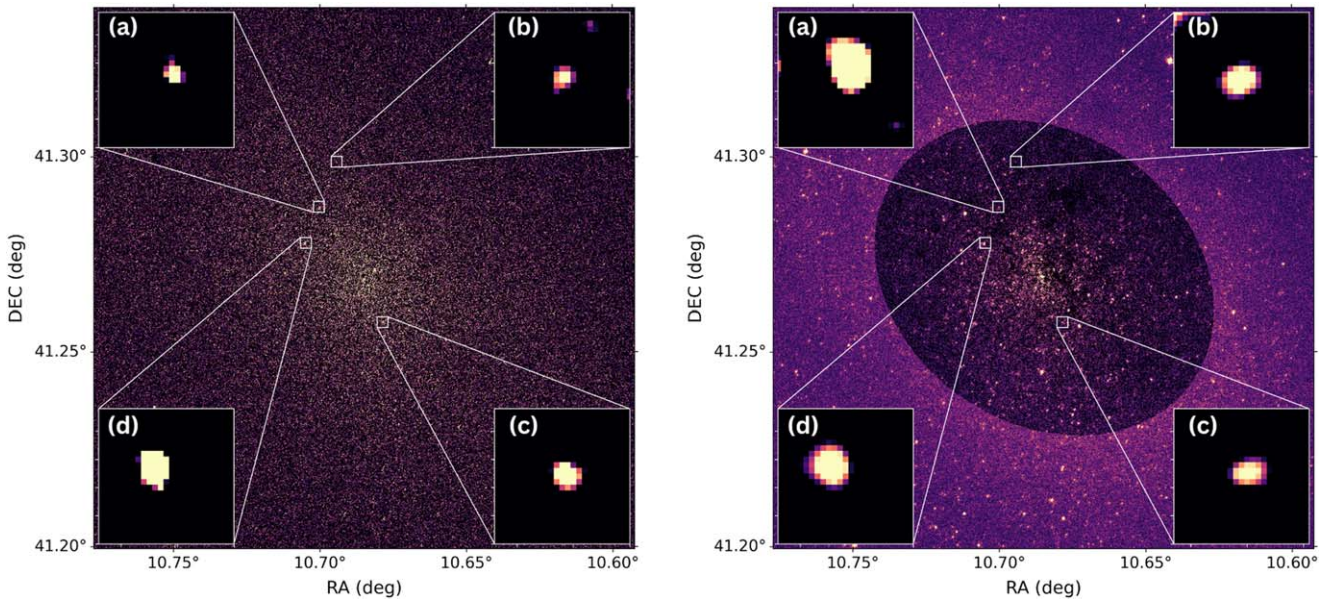

Figure 2. Difference images with inset showing detection of novae (a) M31N 2016-03e, (b) M31N 2015-05a, (c) M31N 2016-05b, and (d) M31N 2016-03c. Left: median-combined template subtraction method. Right: isophote model subtraction method.

pre-outburst, and 2019-12b was detected both before and after the outburst. The quiescent F148W AB magnitudes of novae vary from 21.5 to 24 mag. Depending on the mass of the WD and accretion rate, the contribution in this filter could be due to both the WD and the disk. The quiescent magnitude also strongly depends on the system's orbital inclination (Warner 2008).

The light curve of nova 2019-12b (middle panel in Figure 3) shows a variability in the F148W filter, notably a dip of ∼0.5 mag around 28 days before the eruption. Zamanov et al. (2023) pointed out that dips in light curves are caused by the accumulation of an optically thick, dense shell surrounding the WD prior to the nova eruption. Pre-eruption dips of around 1 mag have been noticed in

Table 2
List of M31 Novae Detected in UVIT Images and Their F148W Mag

Name M31N	R.A. (hh:mm:ss)	Decl. (dd:mm:ss)	Discovery Date (JD)	Observation Date (JD)	Mag (F148W) (AB mag)	Class (Phase)	t_2 (days)	References
Detected at Post-outburst Quiescence								
2015-02a[a]	00:42:33.06	+41:13:08.90	2457047.810	2457671.8566	23.27 ± 0.24	Fe II	⋯	(1–3)
2015-10b[a]	00:43:15.34	+41:20:16.60	2457321.460	2457671.8566	22.54 ± 0.13	Fe II	100.3 ± 75.8 (R)	(4, 5, 75)
2016-02b	00:44:37.03	+41:42:26.40	2457430.370	2457430.3700	22.01 ± 0.12	Fe II	⋯	(6)
2016-03b	00:42:19.51	+41:11:13.70	2457446.280	2457671.8567	22.16 ± 0.14	Nova	41.5 ± 7.1 (R)	(67, 68, 75)
1994-09b	00:42:58.52	+41:15:49.80	2449622.800	2457671.8566	21.88 ± 0.13	⋯	⋯	(32)
2010-12b	00:42:31.08	+41:27:20.30	2455540.620	2457671.8566	21.64 ± 0.09	⋯	3(*R*)[d]	(33, 34)
2013-10c	00:43:09.32	+41:15:41.60	2456574.800	2457671.8566	24.32 ± 0.30	Nova	5.5 ± 1.7 (R)	(35, 36, 75)
2015-12d	00:43:07.79	+41:22:19.30	2457387.220	2457671.8566	21.72 ± 0.10	⋯	⋯	⋯
2018-12a	00:42:40.65	+41:11:08.00	2458455.320	2458788.0143	23.31 ± 0.14	Fe II	⋯	(39–42)
2018-12d	00:43:24.62	+41:20:22.30	2458474.090	2458788.0143	23.33 ± 0.12	Nova	⋯	(42, 43)
2019-06b	00:42:41.73	+41:17:53.70	2458661.560	2458788.0143	22.75 ± 0.14	⋯	⋯	(44)
2019-07c[a]	00:43:00.90	+41:19:19.40	2458672.510	2458788.0143	21.53 ± 0.06	⋯	⋯	(45)
2019-08b	00:44:18.25	+41:32:47.20	2458725.440	2459167.9797	22.00 ± 0.08	Fe II	>57(r'), >53(g')[d]	(46, 47)
2015-05a	00:42:46.60	+41:17:55.3	2457153.56	2457671.8566	23.66 ± 0.31	Nova	⋯	(69, 70)
2016-03c	00:42:49.14	+41:16:40.1	2457430.24	2457671.8566	21.85 ± 0.13	Nova	⋯	(71, 68)
2016-03e	00:42:48.05	+41:17:13.4	2457464.27	2457671.8566	22.78 ± 0.18	⋯	⋯	(72)
2016-05b	00:42:42.88	+41:15:27.4	2457536.55	2457671.8566	22.89 ± 0.29	Fe II	⋯	(68, 73, 74)
2017-06g	00:46:17.94	+41:56:26.1	2457922.69	2458061.9118	20.87 ± 0.12	⋯	⋯	(76)
Detected at Post-outburst Quiescence in Coadded Frames[e]								
1985-09c	00:42:44.50	+41:17:35.0	2446320.74	2458550.6090	23.24 ± 0.10	⋯	⋯	(77)
1998-09e	00:42:49.53	+41:16:47.9	2451083.28	2458550.6090	23.02 ± 0.09	⋯	⋯	(78)
2010-03a	00:42:47.74	+41:17:01.4	2455257.25	2458550.6090	23.18 ± 0.10	Nova	⋯	(79, 80)
Detected at Pre-outburst Quiescence								
2019-12b	00:42:20.47	+41:15:00.00	2458833.090	2457671.8566	23.42 ± 0.25	Fe II	50(r'), 27(g')[d]	(60–62)
2021-07d	00:42:00.58	+41:08:48.30	2459420.380	2458788.0143	22.99 ± 0.13	⋯	⋯	⋯
2019-11f[b]	00:42:51.76	+41:11:26.60	2458814.160	2457671.8566	22.95 ± 0.21	⋯	⋯	(59)
2020-10b[b]	00:42:30.67	+41:21:28.50	2459127.230	2457671.8566	22.15 ± 0.13	⋯	⋯	(63, 64)
2020-10d[b]	00:42:36.20	+41:20:35.50	2459101.180	2457671.8566	23.12 ± 0.20	⋯	⋯	(65)
Detected during Outburst								
2016-08b[a]	00:41:56.82	+41:11:27.60	2457611.050	2457671.8566	20.71 ± 0.12	⋯	42.6 ± 4.3 (R)	(7, 8, 75)
2016-08e	00:43:53.29	+41:26:21.60	2457630.420	2457704.1355	20.83 ± 0.06	Fe II	60.6 ± 16.7 (R)	(9, 10, 75)
2016-09a	00:42:55.66	+41:19:14.50	2457654.300	2457671.8566	23.56 ± 0.22	Fe II	57.0 ± 35.1 (R)	(11, 12, 75)
2016-09b	00:42:17.29	+41:09:44.40	2457657.660	2457671.8566	21.18 ± 0.09	Fe II	43.9 ± 17.3 (R)	(13–15, 75)
2018-05a	00:45:34.90	+41:57:40.40	2458246.700	2458292.3095	20.84 ± 0.12	⋯	⋯	(16)
2019-11a	00:42:30.37	+41:03:29.50	2458789.760	2458805.2565	22.92 ± 0.15	Nova	49(r')[d]	(17, 18)
2020-09b	00:42:46.30	+41:13:35.50	2459117.200	2459174.7140	23.36 ± 0.18	Fe IIb	⋯	(19, 20)
2020-09c	00:43:08.38	+41:08:50.00	2459121.790	2459174.7140	21.64 ± 0.08	Fe II	17(r'), 15(g')[d]	(21, 22)
2020-10f	00:42:20.17	+41:14:28.00	2459154.530	2459174.7140	20.74 ± 0.05	Nova	⋯	(23–25)
2020-11a	00:42:46.79	+41:07:03.10	2459155.080	2459174.7140	21.82 ± 0.09	Nova	⋯	(26, 27)
2020-11c	00:43:13.15	+41:24:56.00	2459159.240	2459174.7140	19.05 ± 0.03	Fe IIb	20(r')[d]	(28–31)
2019-09b	00:42:42.32	+41:17:45.80	2458740.280	2458788.0143	21.72 ± 0.07	He/N	⋯	(48–50)
2019-10c[a]	00:43:01.56	+41:17:59.60	2458776.280	2458788.0143	21.09 ± 0.05	Fe II	18(r'), >22(g')[d]	(54–58)
2021-03a	00:42:34.49	+41:17:29.80	2459188.680	2459174.7140	22.89 ± 0.15	⋯	⋯	(66)
2018-08b	00:39:21.90	+40:15:48.80	2458344.080	2458435.0755	20.92 ± 0.10	Fe II	⋯	(37, 38)
2019-10a[c]	00:42:23.53	+41:11:52.20	2458759.300	2458788.0143	21.78 ± 0.08	Nova	>18(r'), >29(g')[d]	(51–53)

Notes.
[a] Also reported by Leahy et al. (2021).
[b] Also detected around the outburst (within ∼100 days after outburst and ∼10 days before the outburst).
[c] Also detected at quiescence (more than 100 days after the outburst or 30 days before the outburst).
[d] t_2 determined from linear interpolation of the optical data around ($m_{\max} - 2$).
[e] Observation date for coadded images is the midpoint of the first and last observation.

References. (1) Ovcharov et al. (2015a), (2) Fabrika et al. (2015), (3) Delvaux et al. (2015), (4) Williams & Darnley (2015a), (5) Williams & Darnley (2015b), (6) Darnley & Williams (2016a), (7) Kasliwal & Cao (2018a), (8) Hornoch & Kucakova (2016a), (9) Hornoch & Kucakova (2016b), (10) Fabrika et al. (2016c), (11) Hornoch et al. (2016c), (12) Fabrika et al. (2016a), (13) Hornoch & Kucakova (2016c), (14) Valcheva et al. (2016), (15) Fabrika et al. (2016b), (16) Conseil (2018), (17) Campaner 2019, (18) Soraisam et al. (2019b), (19) Zhang & Gao (2020a), (20) Williams et al. (2020a), (21) Hornoch & Kucakova (2020a), (22) Williams et al. (2020c), (23) Zhang & Gao (2020b), (24) Valcheva et al. (2020), (25) Soraisam et al. (2020), (26) Zhang & Gao (2020c), (27) Srivastav et al. (2020), (28) Belligoli (2020), (29) Fabrika et al. (2020), (30) Balcon (2020), (31) Hornoch & Kucakova (2020b), (32) Tomaney & Crotts (1996), (33) Pietsch et al. (2010a), (34) Cao et al. (2012), (35) Ovcharov et al. (2013), (36) Hornoch et al. (2013), (37) Kasliwal & Cao (2018b), (38) Darnley et al. (2018), (39) Zhang & Gao (2018a), (40) Valcheva et al. (2018), (41) Hornoch & Kucakova (2018), (42) Williams et al. (2019a), (43) Zhang & Gao (2018b), (44) Hornoch & Kusnirak (2019), (45) Hornoch & Kucakova (2019a), (46) Conseil (2019), (47) Williams et al. (2019b), (48) Hornoch & Kucakova (2019b), (49) Zhang & Gao (2019a), (50) Lee et al. (2019), (51) Carey (2019), (52) Dahiwale & Fremling (2020), (53) Soraisam et al. (2019a), (54) Nordin et al. (2019), (55) Hornoch & Kucakova (2019c), (56) Madrigal-Aguado et al. (2019), (57) Williams et al. (2019c), (58) Fabrika et al. (2019), (59) Zhang & Gao (2019b), (60) Jiang et al. (2019), (61) Hornoch et al. (2019), (62) Williams et al. (2020b), (63) Zhang & Gao (2020d), (64) Hornoch & Kucakova (2020c), (65) Zhang & Gao (2020e), (66) Fremling (2020), (67) Hornoch & Kucakova (2016d), (68) Martin et al. (2018), (69) Hornoch & Honkova (2015), (70) Ovcharov et al. (2015b), (71) Hornoch et al. (2016a). (72) Hornoch et al. (2016b), (73) Hornoch & Kucakova (2016e), (74) Darnley & Williams (2016b), (75) Clark et al. (2024), (76) Shumkov et al. (2017), (77) Ciardullo et al. (1987), (78) Sharov et al. (2000), (79) Pietsch et al. (2010b), (80) Hornoch et al. (2010).

For more references, check https://www.mpe.mpg.de/~m31novae/opt/m31/M31_table.html.

Table 3
Photometric Data of the UVIT-detected M31 Novae

Name M31N	R.A. (deg)	Decl. (deg)	Discovery (JD)	Observation (JD)	Δt (days)	Filter	Mag (mag)	Limit (mag)
2016-08b	10.48675	41.19100	2457611.05	2457671.85662	60.80662	F148W	20.71 ± 0.13	99
2016-08b	10.48675	41.19100	2457611.05	2457672.19496	61.14496	F172M	20.24 ± 0.22	99
2016-08b	10.48675	41.19100	2457611.05	2457671.85657	60.80657	N219M	20.76 ± 0.11	99
2016-08b	10.48675	41.19100	2457611.05	2457672.19491	61.14491	N279N	19.01 ± 0.11	99

(This table is available in its entirety in machine-readable form in the online article.)

other novae, such as T CrB in optical wavelengths (Schaefer 2023; Maslennikova et al. 2024). If caused by extinction due to an accumulated shell, these dips will be enhanced in the bluer bands. With the available data set, we cannot confirm the maximum drop in magnitude before the eruption. Nonetheless, a drop in FUV magnitude weeks before the eruption hints at the presence of a *pre-eruption dip* in the light curve.

Most other novae detected more than once at post-outburst quiescence in the same filter do not show much variability between epochs. This strengthens the claim of nearly constant flux at quiescence by Selvelli & Gilmozzi (2013). The disks of such systems have steady accretion rates and radiate at constant luminosity.

Among the old novae, only 2010-12b and 1994-09b have been detected at each epoch in multiple filters. Further, three more old novae, 2010-03a, 1998-09e, and 1985-09c, were detected in the coadded images. Detection of these old novae in multiple filters indicates a bright accretion disk. A high accretion rate during quiescence can make the disk brighter. The inclination of the system can also play a major factor in determining if such systems should be so bright long after the eruption. Another factor that could be responsible is the intrinsic brightness of the WD, which illuminates the accretion disk. The FUV flux in the F148W filter could even arise from novae systems with long supersoft source (SSS) phases.

3.2. Novae Detected during Outburst

Fifteen novae were detected within 100 days after the outburst, and five of them were detected within 20 days from the outburst. The only nova detected just before the outburst is 2021-03a, 14 days before its eruption. Most of the novae detected only during outbursts are bright (∼19–20 mag) and fast. Six novae were detected only once in the F148W filter. Four novae were detected in multiple filters, and their SEDs are discussed in Section 3.4.

In the early outburst phase, the photospheric emission is the major source of UV photons. As the photosphere moves inward, the SSS dominates the FUV photon contribution. In the case of partially disrupted disks after eruption, contributions from the inner regions of the accretion disk to the FUV luminosity cannot be ruled out.

3.3. Novae Detected during Quiescence and at Outburst

Four novae were detected both during quiescence and at outburst. 2019-10a was observed in the F148W filter at 46 and 415 days after the outburst, and this indicates a declining trend in its light curve as shown in the top panel of Figure 3.

2019-11f shows a pre-eruption dip similar to that of 2019-12b (see Section 3.1). In the F148W filter, it was observed 1140 and 8 days before the eruption and 360 days after the eruption. Additionally, the pre-eruption dip of 2019-11f is confirmed in the F172M filter observed 1140 and 8 days before the eruption. As shown in the bottom panel of Figure 3, the pre-eruption dip is ∼8 days before the eruption.

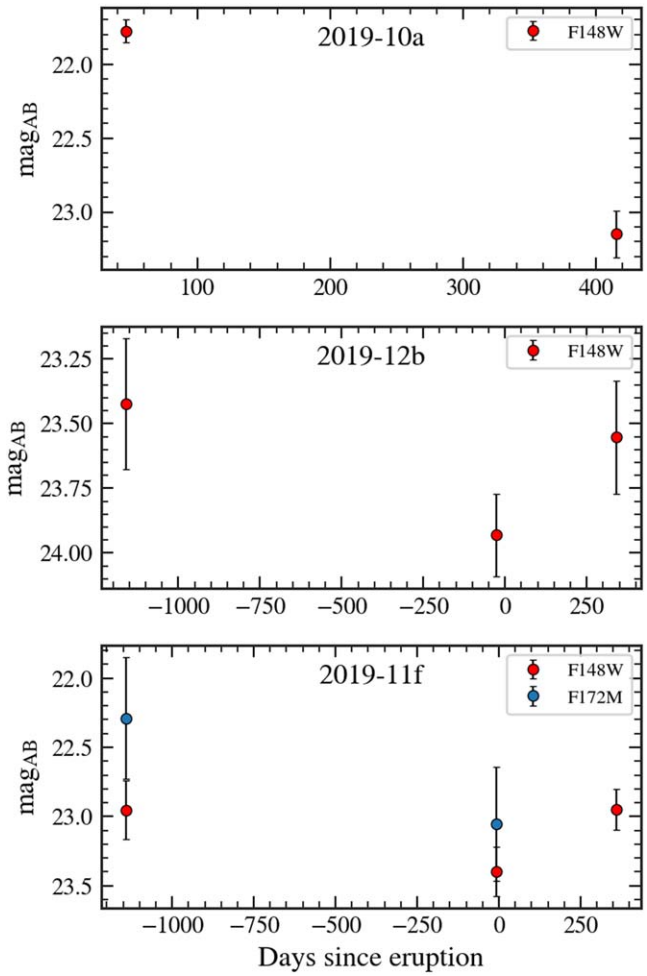

Figure 3. UVIT light curves of some interesting candidates.

The other two novae, 2020-10b and 2020-10d, also show 0.4 and 0.7 mag variability, respectively, but the causes are unclear. However, we would like to point out that these variations are close to the limits of their respective errors.

3.4. The SEDs

Thirteen novae out of the 35 detected have near-simultaneous (within 2 days) observations in multiple filters in the NUV and FUV. These data sets encouraged us to look into their SEDs. The observed SEDs are shown in the top-left

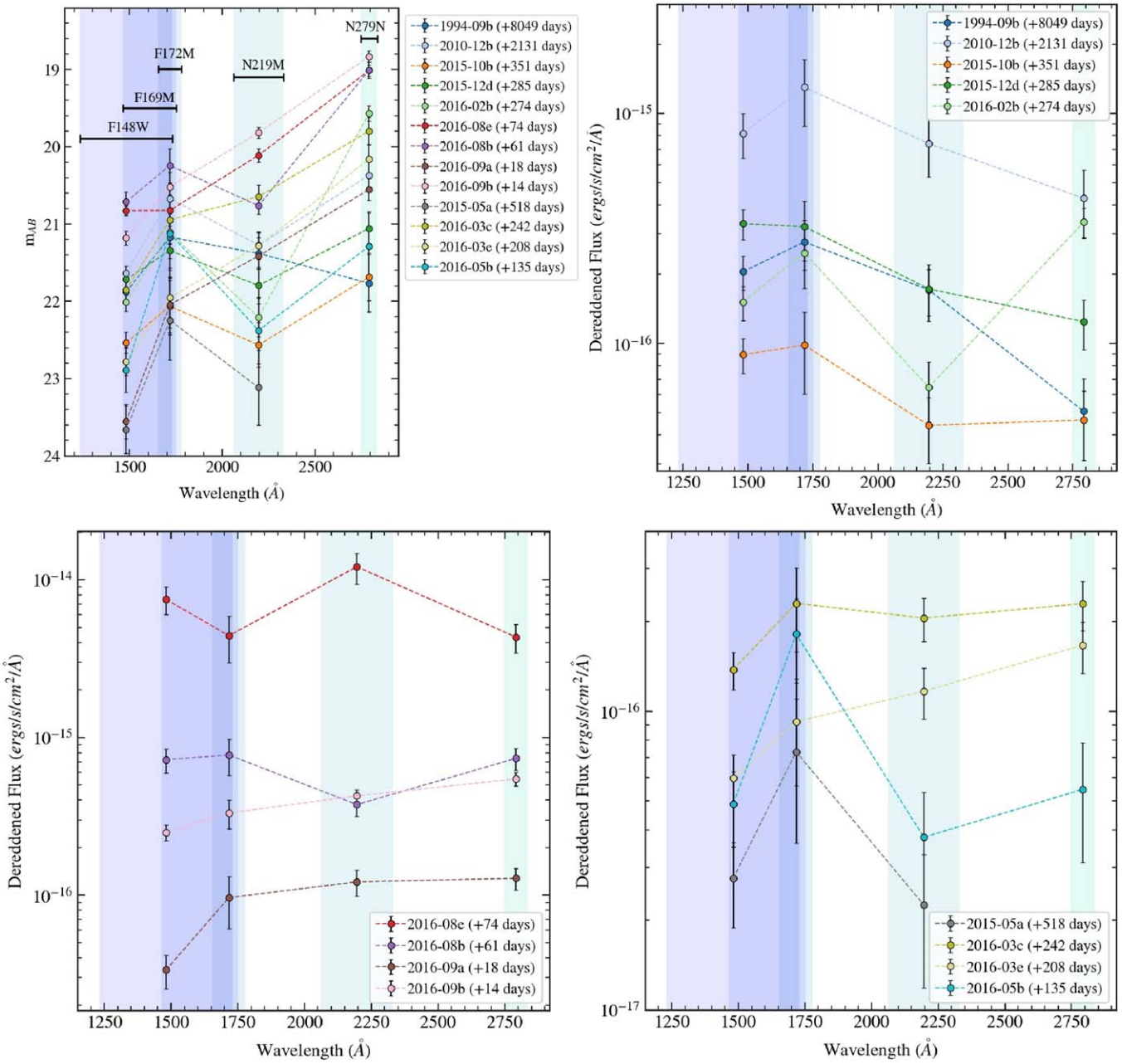

Figure 4. SED of novae detected after outburst are shown in the top-left panel with AB magnitude in the *y*-axis and wavelength in the *x*-axis. The UVIT filter bands are also marked. The extinction-corrected flux of novae detected at post-outburst quiescence (top right), detected close to outburst (bottom left), and detected in the central region (bottom right) are also shown.

subplot of Figure 4. To correct for the extinction toward M31, we derived the A_V values at each nova location from the M160 resolution dust mass maps of Draine et al. (2014), owing to its complete M31 coverage. However, compared to the PHAT survey of Dalcanton et al. (2015), the extinction values were overestimated by a factor of $\sim$2 (B.T. Draine 2024, private communication). The A_V values derived from Draine et al. (2014) were corrected before applying to the SED of each nova. The UVIT AB magnitudes were converted to flux using the relations given in Tandon et al. (2017b). We used the extinction functions from Cardelli et al. (1989) to deredden the UV flux using the `extinction` (Barbary 2021) package in `Python`. The extinction-corrected SEDs in terms of F_λ against λ are shown in Figure 4.

The most interesting candidates are those detected at post-outburst quiescence, shown in the upper-right panel of Figure 4. The power-law dependence of $F_\lambda \propto \lambda^{-\alpha}$ was fitted to obtain the best-fit power laws given in Table 4. The radiation from accretion disks follows a power law with a slope of $\alpha = 7/3$. The best-fit α values for the novae are within the error bars of this, indicating the presence of accretion disks (Frank et al. 2002). This confirms that most of the UV radiation originates from the accretion disk at quiescence (Selvelli & Gilmozzi 2013). Another point to note is that the flux in the F148W filter is comparatively less than that in F172M. This could indicate that blueward of 1600 Å, the flux from the disk starts to diminish and could have a contribution from the WD's blackbody tail.

Table 4
α Values of Novae with Accretion Disk Signatures

M31N	α	α_2
1994-09b	2.71 ± 0.81	3.28 ± 0.79
2010-12b	2.29 ± 0.01	2.29 ± 0.94
2015-10b	2.01 ± 0.96	1.34 ± 1.32
2015-12d	2.15 ± 0.33	1.92 ± 0.82

Note. α corresponds to the power law between F_λ versus λ when errors in A_V are not taken into account, whereas α_2 corresponds to the same power law when errors in A_V are taken into account.

Four novae were caught during their eruption in multiple filters, and their SEDs are shown in the lower-left panel of Figure 4. Two novae, 2016-09a and 2016-09b, were observed within 18 days of eruption. Their speed class suggests that they belong to a moderately fast category, and both were also confirmed to be in their Fe II phase (see Table 2). Their SEDs indicate an increasing flux from the FUV to the NUV, hinting at the peak being in the optical region. The peak brightness of the nova eruption corresponds to the maximum extent of the photosphere. During the maxima, the peak of the SED moves to longer wavelengths, which could be in the UV for very fast novae but also in the optical or even the IR for slow novae. As the photosphere recedes, hotter regions closer to the WD are revealed, and the SED peak moves blueward. A SED with its peak in optical bands could indicate that these two novae were observed at a stage when their pseudo-photosphere was shrinking.

The SEDs of the novae 2016-02b, 2016-08e, and 2016-08b deviate from the power law expected from accretion disks. One possible cause for this could be the presence of spectral features in the UV bands. The quiescent novae sample of Selvelli & Gilmozzi (2013) consisted majorly of C IV 1550 Å, along with some fainter features like N V 1240 Å, Si IV 1400 Å, He II 1640 Å, O III] 1666 Å, and N III] 1750 Å in emission. FUV absorption features arising from metals such as Si II 1190 Å, Si II 1260 Å, O I+Si II 1303 Å, C II 1335 Å, Si IV 1400 Å, C IV 1550 Å, and N V 1240 Å can also distort the SEDs. During the outburst, however, the UV spectral features are mostly emission until the Fe curtains stage sets in. The list of emission lines and how they evolve have been described in Shore (2008).

Another possibility for the deviation of the SED could be the inaccurate determination of the extinction parameter, which would amplify any errors in the FUV bands as well as in the N219M band (since it covers the UV extinction bump at 2175 Å). The SED of the quiescent nova 2016-02b could be undercorrected for extinction. The SED of 2016-08e might be overcorrected, whereas that of 2016-08b might have been undercorrected, both of which were captured during the outburst. The overcorrection in some of the SEDs of novae could imply that the sources are away from the galaxy's disk toward us, i.e., these sources suffer less extinction than predicted by the dust maps. Similarly, sources with undercorrection may be located on the far side of M31, thus suffering more extinction than obtained from the dust maps.

The bulge of M31 in FUV is complicated. Leahy et al. (2023) could fit the bulge with a single component but showed that an eight-component model fits best. Such a complicated bulge region will lead to contamination, dependent on the spatial location of the novae and on the different UV wave bands. Furthermore, the location of these novae inside the nuclear region is unknown, leading to uncertainties in determining their column densities and extinction. It thus becomes difficult to extract much information from the SEDs of novae in the central region of M31.

4. Summary and Conclusion

Astronomers have extensively studied novae in M31, in the optical for more than a century, and in X-rays over the last couple of decades to understand their distribution, rates, and evolution at different phases. However, UV surveys remain limited. This study utilizes multiband AstroSat UV data to explore cataclysmic variables, novae in particular, during outbursts and quiescence. Below, we present the key findings from our investigation.

1. We have examined 91 sets of UVIT images of M31 from 2016 onward, uncovering at least one nova in 19 of those images. Over 80% of the identified novae were situated within or close to the central bulge.
2. We employed two image subtraction methods to eliminate the light from the galactic bulge, leading to the detection of four novae previously obscured by the brightness of the central region of M31.
3. A total of 42 novae were identified, with 15 observed across multiple filters in both the FUV and the NUV. Additionally, several novae were detected in multiple epochs. Magnitude upper limits were estimated for more than 1000 novae undetected in individual and coadded frames.
4. During quiescence, the SEDs of novae exhibit indications of the accretion disk's influence, confirming its dominance in UV radiation during this phase. Analysis of the SEDs of two novae during outburst indicates they were observed while their photospheres were receding.
5. The FUV light curves of two novae exhibit a pre-eruption dip that can possibly be attributed to the accumulation of accreted material in a shell before the nova eruption. Multiepoch photometry of the novae at quiescence indicates a near-constant magnitude, a sign of a steady accretion rate.

Upcoming UV missions like INSIST (Subramaniam 2022), CASTOR (Côte et al. 2012), UVEX (Kulkarni et al. 2021), and ULTRASAT (Shvartzvald et al. 2024) offer the potential for detecting novae at different stages of their UV evolution. These observations can provide insights into disk activity, accretion processes, and the characteristics of the WD during dormancy phases. Additionally, by employing high-frequency observations, we anticipate elucidating the UV flash preceding eruptions, as predicted by the theoretical models of Kato et al. (2022), along with the rapid UV evolution post-outburst. We have initiated a UV survey of M31's central region using the FUV F148W filter on UVIT/AstroSat. Initial observations have revealed the detection of the newly identified RN M31N 2013-10c during our monitoring activities (Basu et al. 2024a). The FUV survey was designed to complement the simultaneous monitoring of M31 by the GROWTH-India Telescope (GIT; Kumar et al. 2022) in g', r' bands, which has detected numerous novae and even discovered the nova AT 2023tkw

(GIT230919aa, Kumar 2023). The integration of UV monitoring with multiwavelength surveys such as the Zwicky Transient Facility (ZTF; Bellm et al. 2019) and GIT in the optical, XRISM in X-rays (XRISM Science Team 2020), and the forthcoming Roman Space Telescope in the IR (Akeson et al. 2019), alongside Daksha in X-rays (Bhalerao et al. 2024), promises to contribute significantly to resolving outstanding questions concerning nova phenomena.

Acknowledgments

We appreciate the anonymous reviewer's insightful comments and suggestions, which have enhanced the quality of this article. This work uses the archival UVIT data from the AstroSat mission of the Indian Space Research Organisation (ISRO). We thank the PIs of the proposals that were observed. The proposal IDs are the first seven characters of the observation IDs given in Table 1. We thank the UVIT payload operation centers for verifying and releasing the raw and processed data via the ISSDC data archive and providing the necessary software tools. G.C.A. thanks the Indian National Science Academy for support under the INSA Senior Scientist Programme. K.S. thanks the Indian Institute of Astrophysics for supporting her work while at IIA.

Facility: AstroSat (UVIT).

Software: `CCDLAB` (Postma & Leahy 2017), `IRAF v2.16.1` (Tody 1993), `Python v3.6.6` (Van Rossum & Drake 2009), `NumPy` (Harris et al. 2020), `SciPy` (Virtanen et al. 2020), `Pandas` (McKinney et al. 2010), `Matplotlib` (Hunter 2007), `photutils` (Bradley et al. 2023), `SWarp` (Bertin et al. 2002), `SAOImageDS9` (Joye & Mandel 2003).

Appendix
Catalog Table

The UVIT catalog with detection magnitudes and nondetection limits of all M31 novae is provided in Table 5.

Table 5
UVIT Catalog of all M31 Novae Detections and Nondetections in Each Filter, Along with Available Archival Data

Name M31N	R.A. (hh:mm:ss)	Decl. (dd:mm:ss)	UVIT Field	Individual Detection[a]	Discovery Date (JD)	Max (mag)	Filter	t_2 (days)	Alternative Names	F148W mag (AB mag)	F172M mag (AB mag)	F169M mag (AB mag)	N219M mag (AB mag)	N279N mag (AB mag)
2022-04d	00:38:48.05	+40:15:26.7	15	N	2459695.52	16.5	*w*	⋯	AT2022iro	> 23.34	⋯	> 24.30	⋯	⋯
2022-04c	00:42:57.33	+41:16:18.4	1	N	2459692.41	17.3	*w*	⋯	AT2022icc	> 23.31	> 22.29	> 22.67	> 21.86	> 21.05
2021-07d	00:42:00.58	+41:08:48.3	1	Y	2459420.38	19.3	*w*	⋯	XM57MZ	23.21 ± 0.09	23.76 ± 0.32	22.40 ± 0.17	> 22.08	> 21.53
2021-07c	00:42:17.92	+41:00:18.5	3	N	2459399.89	18.3	*r*	⋯	AT2021scd, ZTF21abjiotr	> 22.83	> 22.07	⋯	> 22.36	> 21.87
2020-10f	00:42:20.17	+41:14:28.0	1	Y	2459154.53	16.3	*R*	⋯	AT2020yky, XM42MZ	21.99 ± 0.042	> 23.12	> 22.63	> 22.08	> 21.48
2020-10e	00:42:37.35	+41:20:52.2	1	N	2459144.24	16.3	*R*	4	AT2020xyv, XM41MZ	> 24.02	> 23.18	> 22.63	> 22.08	> 21.53
2020-01b	00:42:52.34	+41:16:13.1	1	N	2458877.04	17.40 ± 0.15	*R*	11.4 ± 2.5	AT2020ber, XM24MZ	> 22.96	> 22.37	> 22.60	> 21.61	> 20.68
2017-06g	00:46:17.94	+41:56:26.1	8	Y	2457922.69	18.1	*w*	⋯	MASTER OT J004617.94 +415626.1	21.89 ± 0.10	> 23.28	⋯	> 22.06	20.70 ± 0.18
2016-11b	00:42:42.81	+41:12:33.4	1	N	2457720.26	16.03 ± 0.05	*R*	12.6 ± 1.8	PNV J00424281 +4112334	> 23.53	> 22.91	> 22.59	> 22.08	> 21.53
2016-03e	00:42:48.05	+41:17:13.4	1	Y	2457464.27	16.9	*w*	⋯	PNV J00424805 +4117134	23.98 ± 0.21	23.59 ± 0.52	> 22.15	21.28 ± 0.18	20.16 ± 0.18

Notes. The UVIT magnitudes were estimated from the coadded images where more than one epoch of data was available in the same field and filter. In other cases, magnitudes were estimated from the individual frames. The fields with an ellipsis (⋯) in the UVIT magnitude columns indicate the absence of data for that field in that filter.
[a] Y indicates detection in at least one individual frame. N indicates nondetection in individual frames.

(This table is available in its entirety in machine-readable form in the online article.)

ORCID iDs

Judhajeet Basu https://orcid.org/0000-0001-7570-545X
Krishnendu S. https://orcid.org/0009-0009-8534-9765
Sudhanshu Barway https://orcid.org/0000-0002-3927-5402
Shatakshi Chamoli https://orcid.org/0009-0000-5909-293X
G. C. Anupama https://orcid.org/0000-0003-3533-7183

References

Akeson, R., Armus, L., Bachelet, E., et al. 2019, arXiv:1902.05569
Arp, H. C. 1956, AJ, 61, 15
Aydi, E., Page, K. L., Kuin, N. P. M., et al. 2018, MNRAS, 474, 2679
Aydi, E., Sokolovsky, K. V., Chomiuk, L., et al. 2020, NatAs, 4, 776
Balcon, C. 2020, Transient Name Server Classification Report 2020-2051
Barbary, K., 2021 Extinction: Dust extinction laws, Astrophysics Source Code Library v.0.4.6, ascl:2102.026
Basu, J., Chamoli, S., Barway, S., & Anupama, G. 2024a, ATel, 16526
Basu, J., Pavana, M., Anupama, G. C., et al. 2024b, ApJ, 966, 44
Belligoli, R. 2020, Transient Name Server Discovery Report 2020-709
Bellm, E. C., Kulkarni, S. R., Graham, M. J., et al. 2019, PASP, 131, 018002
Bertin, E., Mellier, Y., Radovich, M., et al. 2002, in ASP Conf. Ser. 281, Astronomical Data Analysis Software and Systems XI, ed. D. A. Bohlender, D. Durand, & T. H. Handley (San Francisco, CA: ASP), 228
Bhalerao, V., Sawant, D., Pai, A., et al. 2024, ExA, 57, 23
Bode, M. F., Darnley, M. J., Beardmore, A. P., et al. 2016, ApJ, 818, 145
Bode, M. F., & Evans, A. 2008, Classical Novae (Cambridge: Cambridge Univ. Press)
Bradley, L., Sipőcz, B., Robitaille, T., et al. 2023, astropy/photutils: v1.8.0, Zenodo, doi:10.5281/zenodo.7946442
Campaner, P. 2019, Transient Name Server Discovery Report 209-23011
Cao, Y., Kasliwal, M. M., Neill, J. D., et al. 2012, ApJ, 752, 133
Cardelli, J. A., Clayton, G. C., & Mathis, J. S. 1989, ApJ, 345, 245
Carey, G. 2019, Transient Name Server Discovery Report 2019-1970
Chomiuk, L., Metzger, B. D., & Shen, K. J. 2021, ARA&A, 59, 391
Ciardullo, R., Ford, H. C., Neill, J. D., Jacoby, G. H., & Shafter, A. W. 1987, ApJ, 318, 520
Clark, J. G., Hornoch, K., Shafter, A. W., et al. 2024, arXiv:2404.04733
Conseil, E. 2018, Transient Name Server Discovery Report 2018-597
Conseil, E. 2019, Transient Name Server Discovery Report 2019-1718
Côte, P., Scott, A., Balogh, M., et al. 2012, Proc. SPIE, 8442, 844215
Dahiwale, A., & Fremling, C. 2020, Transient Name Server Classification Report 2020-2139
Dalcanton, J. J., Fouesneau, M., Hogg, D. W., et al. 2015, ApJ, 814, 3
Darnley, M. J., Bode, M. F., Kerins, E., et al. 2004, MNRAS, 353, 571
Darnley, M. J., Bode, M. F., Kerins, E., et al. 2006, MNRAS, 369, 257
Darnley, M. J., Healy, M. W., & Williams, S. C. 2018, ATel, 11983
Darnley, M. J., & Williams, S. C. 2016a, ATel, 8710
Darnley, M. J., & Williams, S. C. 2016b, ATel, 9143
Delvaux, C., Greiner, J., & Pietsch, W. 2015, ATel, 7104
Devaraj, A., Joseph, P., Stalin, C. S., Tandon, S. N., & Ghosh, S. K. 2023, ApJ, 946, 65
Draine, B. T., Aniano, G., Krause, O., et al. 2014, ApJ, 780, 172
Fabrika, S., Barsukova, E. A., Valeev, A. F., et al. 2015, ATel, 7158
Fabrika, S., Sholukhova, O., Sarkisyan, A., et al. 2020, ATel, 14217
Fabrika, S., Sholukhova, O., Solovyeva, Y., et al. 2019, ATel, 13230
Fabrika, S., Sholukhova, O., Valeev, A. F., et al. 2016a, ATel, 9557
Fabrika, S., Sholukhova, O., Valeev, A. F., et al. 2016b, ATel, 9563
Fabrika, S., Sholukhova, O., Valeev, A. F., et al. 2016c, ATel, 9443
Frank, J., King, A., & Raine, D. 2002, Accretion Power in Astrophysics (Cambridge: Cambridge Univ. Press)
Fremling, C. 2020, Transient Name Server Discovery Report 2020-3674
Gehrz, R. D., Truran, J. W., Williams, R. E., & Starrfield, S. 1998, PASP, 110, 3
Guo, Y., Wu, C., & Wang, B. 2022, A&A, 660, A53
Hachisu, I., & Kato, M. 2006, ApJS, 167, 59
Harris, C. R., Millman, K. J., van der Walt, S. J., et al. 2020, Natur, 585, 357
Henze, M., Pietsch, W., Haberl, F., et al. 2010, A&A, 523, A89
Henze, M., Pietsch, W., Haberl, F., et al. 2011, A&A, 533, A52
Henze, M., Pietsch, W., Haberl, F., et al. 2014, A&A, 563, A2
Hernanz, M., & Jose, J. 1998, in ASP Conf. Ser. 137, Wild Stars in the Old West, ed. S. Howell, E. Kuulkers, & C. Woodward (ASP: San Francisco, CA), 368
Hillman, Y., Prialnik, D., Kovetz, A., & Shara, M. M. 2016, ApJ, 819, 168
Hornoch, K., & Honkova, K. 2015, ATel, 7492
Hornoch, K., & Kucakova, H. 2016a, ATel, 9373
Hornoch, K., & Kucakova, H. 2016b, ATel, 9431
Hornoch, K., & Kucakova, H. 2016c, ATel, 9552
Hornoch, K., & Kucakova, H. 2016d, ATel, 8785
Hornoch, K., & Kucakova, H. 2016e, ATel, 9098
Hornoch, K., & Kucakova, H. 2018, ATel, 12262
Hornoch, K., & Kucakova, H. 2019a, ATel, 12925
Hornoch, K., & Kucakova, H. 2019b, ATel, 13109
Hornoch, K., & Kucakova, H. 2019c, ATel, 13207
Hornoch, K., & Kucakova, H. 2020a, ATel, 14055
Hornoch, K., & Kucakova, H. 2020b, ATel, 14155
Hornoch, K., & Kucakova, H. 2020c, ATel, 14068
Hornoch, K., Kucakova, H., & Wolf, M. 2016a, ATel, 8787
Hornoch, K., Kucakova, H., & Wolf, M. 2019, ATel, 13355
Hornoch, K., & Kusnirak, P. 2019, ATel, 12895
Hornoch, K., Kubanek, P., Morales, N., et al. 2010, CBET 2192
Hornoch, K., Manilla-Robles, A., Tudor, V., Vaduvescu, O., & Ramsay, G. 2013, ATel, 5503
Hornoch, K., Vrastil, J., Honkova, K., & Kucakova, H. 2016b, ATel, 8877
Hornoch, K., Wolf, M., & Kucakova, H. 2016c, ATel, 9545, 1
Hunter, J. D. 2007, CSE, 9, 90
Jiang, X., Sun, G., Zhang, M., & Gao, X. 2019, Transient Name Server Discovery Report 2019-2620
Joye, W. A., & Mandel, E. 2003, in ASP Conf. Ser. 295, Astronomical Data Analysis Software and Systems XII, ed. H. E. Payne, R. I. Jedrzejewski, & R. N. Hook (San Francisco, CA: ASP), 489
Kasliwal, M., & Cao, Y. 2018a, Transient Name Server Discovery Report 2018-1344
Kasliwal, M., & Cao, Y. 2018b, Transient Name Server Discovery Report 2018-1069
Kasliwal, M. M., Cenko, S. B., Kulkarni, S. R., et al. 2011, ApJ, 735, 94
Kato, M., Saio, H., & Hachisu, I. 2022, PASJ, 74, 1005
Kraft, R. P. 1964, ApJ, 139, 457
Kuin, N. P. M., Page, K. L., Mróz, P., et al. 2020, MNRAS, 491, 655
Kulkarni, S. R., Harrison, F. A., Grefenstette, B. W., et al. 2021, arXiv:2111.15608
Kumar, H., Bhalerao, V., Anupama, G. C., et al. 2022, AJ, 164, 90
Kumar, R. 2023, Transient Name Server Discovery Report 2023-2354
Leahy, D., Buick, M., Postma, J., & Morgan, C. 2021, AJ, 161, 215
Leahy, D., Craiciu, T., & Postma, J. 2023, ApJS, 265, 6
Leahy, D. A., Postma, J., Chen, Y., & Buick, M. 2020, ApJS, 247, 47
Lee, C. H., Riffeser, A., Seitz, S., et al. 2012, A&A, 537, A43
Lee, C.-H., Soraisam, M., Narayan, G., Matheson, T., & Saha, A. 2019, ATel, 13141
Lessing, A. M., Shara, M. M., Hounsell, R., et al. 2023, arXiv:2309.16856
Madrigal-Aguado, A., Alvarez-Hernandez, L., Bayer, J., et al. 2019, ATel, 13272
Martin, T. B., Drissen, L., & Melchior, A.-L. 2018, MNRAS, 473, 4130
Maslennikova, N. A., Tatarnikov, A. M., Tatarnikova, A. A., et al. 2024, AstL, 49, 501
McKinney, W., et al. 2010, in Proc. of the 9th Python in Science Conf, ed. S. van der Walt & J. Millman (Austin, TX: SciPy), 56
Mróz, P., Udalski, A., Poleski, R., et al. 2016, ApJS, 222, 9
Nordin, J., Brinnel, V., Giomi, M., et al. 2019, Transient Name Server Discovery Report 209-2130
Ovcharov, E., Kostov, A., Kurtenkov, A., Valcheva, A., & Nedialkov, P. 2015a, ATel, 7065
Ovcharov, E., Kurtenkov, A., Nikolov, G., et al. 2013, ATel, 5475
Ovcharov, E., Minev, M., Bozhilov, V., et al. 2015b, ATel, 7789
Page, K. L., Beardmore, A. P., & Osborne, J. P. 2020, AdSpR, 66, 1169
Page, K. L., Kuin, N. P. M., & Osborne, J. P. 2022, Univ, 8, 643
Pietsch, W. 2010, AN, 331, 187
Pietsch, W., Haberl, F., Sala, G., et al. 2007, A&A, 465, 375
Pietsch, W., Henze, M., Burwitz, V., et al. 2010a, ATel, 3076
Pietsch, W., Lloyd, J., Henze, M., et al. 2010b, ATel, 2964
Postma, J. E., & Leahy, D. 2017, PASP, 129, 115002
Postma, J. E., & Leahy, D. 2021, JApA, 42, 30
Rector, T. A., Jacoby, G. H., Corbett, D. L., Denham, M. & RBSE Nova Search Team 1999, AAS Meeting, 195, 36.08
Rector, T. A., Shafter, A. W., Burris, W. A., et al. 2022, ApJ, 936, 117
Rosino, L. 1964, AnAp, 27, 498
Rosino, L. 1973, A&AS, 9, 347
Rosino, L., Capaccioli, M., D'Onofrio, M., & della Valle, M. 1989, AJ, 97, 83
Schaefer, B. E. 2023, MNRAS, 524, 3146
Selvelli, P., & Gilmozzi, R. 2013, A&A, 560, A49
Selvelli, P., & Gilmozzi, R. 2019, A&A, 622, A186

Shafter, A. W., Bode, M. F., Darnley, M. J., et al. 2011a, ApJ, 727, 50
Shafter, A. W., Darnley, M. J., Hornoch, K., et al. 2011b, ApJ, 734, 12
Shafter, A. W., & Irby, B. K. 2001, ApJ, 563, 749
Shara, M. M., Lessing, A. M., Hounsell, R., et al. 2023, ApJS, 269, 42
Sharov, A. S., & Alksnis, A. 1991, Ap&SS, 180, 273
Sharov, A. S., Alksnis, A., Zharova, A. V., & Shokin, Y. A. 2000, AstL, 26, 433
Shen, K. J., & Quataert, E. 2022, ApJ, 938, 31
Shore, S. N. 2008, in Classical Novae, ed. M. F. Bode & A. Evans (Cambridge: Cambridge Univ. Press), 194
Shumkov, V., Lipunov, V., Rebolo, R., et al. 2017, ATel, 10506
Shvartzvald, Y., Waxman, E., Gal-Yam, A., et al. 2024, ApJ, 964, 74
Singh, K. P., Tandon, S. N., Agrawal, P. C., et al. 2014, Proc. SPIE, 9144, 91441S
Soraisam, M., Lee, C.-H., Narayan, G., Matheson, T., & Saha, A. 2019a, ATel, 13210
Soraisam, M., Lee, C.-H., Nunez, R., et al. 2019b, ATel, 13317
Soraisam, M., McKinnon, K., Nunez, R., et al. 2020, ATel, 14150
Srivastav, S., Smartt, S. J., McBrien, O., et al. 2020, Transient Name Server Classification Report 2020-3471,
Starrfield, S. 1986, in New Insights in Astrophysics: Eight Years of UV Astronomy with IUE, ed. E. J. Rolfe & R. Wilson (Nordwijk: ESA Publications Division), 379, ESA SP-263
Starrfield, S. 1999, PhR, 311, 371
Starrfield, S., Bose, M., Iliadis, C., et al. 2020, ApJ, 895, 70
Starrfield, S., Iliadis, C., & Hix, W. R. 2016, PASP, 128, 051001
Strope, R. J., Schaefer, B. E., & Henden, A. A. 2010, AJ, 140, 34
Subramaniam, A. 2022, JApA, 43, 80
Subramaniam, A., Tandon, S. N., Hutchings, J., et al. 2016, Proc. SPIE, 9905, 99051F
Tandon, S. N., Hutchings, J. B., Ghosh, S. K., et al. 2017a, JApA, 38, 28
Tandon, S. N., Postma, J., Joseph, P., et al. 2020, AJ, 159, 158
Tandon, S. N., Subramaniam, A., Girish, V., et al. 2017b, AJ, 154, 128
Tody, D. 1993, in ASP Conf. Ser. 52, Astronomical Data Analysis Software and Systems II, ed. R. J. Hanisch, R. J. V. Brissenden, & J. Barnes (San Francisco, CA: ASP), 173
Tomaney, A. B., & Crotts, A. P. S. 1996, AJ, 112, 2872
Tomaney, A. B., & Shafter, A. W. 1992, ApJS, 81, 683
Valcheva, A., Kostov, A., Minev, M., Ovcharov, E., & Nedialkov, P. 2018, ATel, 12261
Valcheva, A., Kurtenkov, A., Ovcharov, E., et al. 2016, ATel, 9559
Valcheva, A., Minev, M., Ovcharov, E., & Nedialkov, P. 2020, ATel, 14212
Van Rossum, G., & Drake, F. L. 2009, Python 3 Reference Manual (Scotts Valley: CA: CreateSpace)
Virtanen, P., Gommers, R., Oliphant, T. E., et al. 2020, NatMe, 17, 261
Wang, B. 2018, RAA, 18, 049
Warner, B. 2008, in Classical Novae, ed. M. F. Bode & A. Evans (Cambridge: Cambridge Univ. Press), 16
Williams, S. C., & Darnley, M. J. 2015a, ATel, 8218
Williams, S. C., & Darnley, M. J. 2015b, ATel, 8281
Williams, S. C., Darnley, M. J., Bode, M. F., Keen, A., & Shafter, A. W. 2014, ApJS, 213, 10
Williams, S. C., Darnley, M. J., Bode, M. F., & Shafter, A. W. 2016, ApJ, 817, 143
Williams, S. C., Darnley, M. J., Healy, M. W., Murphy-Glaysher, F. J., & Ransome, C. L. 2019b, ATel, 13078
Williams, S. C., Darnley, M. J., Healy, M. W., Murphy-Glaysher, F. J., & Ransome, C. L. 2019c, ATel, 13228
Williams, S. C., Darnley, M. J., Healy, M. W., Murphy-Glaysher, F. J., & Ransome, C. L. 2020a, ATel, 14053
Williams, S. C., Darnley, M. J., Healy, M. W., Murphy-Glaysher, F. J., & Ransome, C. L. 2020b, ATel, 13384
Williams, S. C., Darnley, M. J., & Healy, M. W. 2019a, ATel, 12349
Williams, S. C., Darnley, M. J., Healy, M. W., et al. 2020c, ATel, 14121
XRISM Science Team 2020, arXiv:2003.04962
Zamanov, R. K., Marchev, V., Marti, J., & Latev, G. Y. 2023, arXiv:2308.04104
Zhang, M., & Gao, X. 2018a, Transient Name Server Discovery Report 2018-2050
Zhang, M., & Gao, X. 2018b, Transient Name Server Discovery Report 2018-2069
Zhang, M., & Gao, X. 2019a, Transient Name Server Discovery Report 2019-1827
Zhang, M., & Gao, X. 2019b, Transient Name Server Discovery Report 2019-2512
Zhang, M., & Gao, X. 2020a, Transient Name Server Discovery Report 2020-2924
Zhang, M., & Gao, X. 2020b, Transient Name Server Discovery Report 2020-3351
Zhang, M., & Gao, X. 2020c, Transient Name Server Discovery Report 2020-3322
Zhang, M., & Gao, X. 2020d, Transient Name Server Discovery Report 2020-3028
Zhang, M., & Gao, X. 2020e, Transient Name Server Discovery Report 2020-3130